Organization of Oceanic Convection during the Onset of the 1998 East Asian Summer Monsoon

RICHARD H. JOHNSON, STEVEN L. AVES, AND PAUL E. CIESIELSKI

Department of Atmospheric Science, Colorado State University, Fort Collins, Colorado

THOMAS D. KEENAN

Bureau of Meteorology Research Centre, Melbourne, Australia

(Manuscript received 17 February 2004, in final form 12 July 2004)

ABSTRACT

The organizational modes of convection over the northern South China Sea (SCS) during the onset of the summer monsoon are documented using radar and sounding data from the May–June 1998 South China Sea Monsoon Experiment (SCSMEX). The onset occurred in mid-May with a rapid increase in deep convection over a 10-day period, accompanied by a major shift in the circulation over the east Asian region.

Analysis of Bureau of Meteorology Research Centre (BMRC) radar data from Dongsha Island reveals a wide range of organizational modes of convection over the northern SCS. Proximity sounding data indicate that lower- and middle-level vertical wind shears exerted a dominant control over the orientation of convective lines within mesoscale convective systems in this region, as has been found in the Australian monsoon region and the equatorial western Pacific. The results are consistent with the conceptual model of LeMone et al. based on the Tropical Ocean Global Atmosphere Coupled Ocean–Atmosphere Response Experiment (TOGA COARE), except two new organizational modes have been identified: shear-parallel bands for strong low-level shear and weak midlevel shear when there is weak instability and the air is dry aloft, and shear-parallel bands for strong shears in both layers when the shear vectors are in the same direction. Midlatitude influences, namely, the passage of troughs over southern China, likely contributed to these two additional modes.

The stratiform rain fraction from the convective systems during the monsoon onset period was relatively small (26%) compared to the estimated average of about 40% for the entire Tropics. This small fraction is attributed to the weak instability during the onset period and relatively dry air in the upper troposphere.

1. Introduction

The east Asian monsoon (EAM) is characterized by distinctly different winter and summer circulation patterns, with transitions between the two occurring on a relatively rapid time scale. During the winter monsoon, cold air flows southward off mainland China over the South China Sea (SCS), eventually converging into deep convective systems over the Indonesian–Malaysian maritime continent. The structure and properties of convective systems over the southern SCS near Borneo during the winter monsoon were studied by Houze et al. (1981) and Johnson and Kriete (1982). In contrast, the summer monsoon features southwesterly flow of moist air across the SCS feeding deep convective systems over the regions of China, Japan, and Korea. The focus of this paper is on the summer component of the East Asian monsoon. It is during this period that the 1998 South China Sea Monsoon Experiment (SCSMEX; Lau et al. 2000) was conducted, providing new observations of convective systems over the northern SCS around the time of the onset of the EAM. Studies of the large-scale and regional characterisitcs of the flow accompanying the onset of the monsoon during SCSMEX have been recently reported by Chan et al. (2000), Ding and Liu (2001), and Johnson and Ciesielski (2002).

It has long been known that the organization of tropical convection is influenced predominantly by the vertical shear and convective available potential energy or CAPE (Moncrieff and Green 1972). Various observational studies in the eastern tropical Atlantic and northern Australia have confirmed the strong influence of environmental winds on the structure, orientation, and propagation of convective bands (e.g., Barnes and Seickman 1984; Alexander and Young 1992; Keenan and Carbone 1992). Recently, LeMone et al. (1998) inves-

Corresponding author address: Richard H. Johnson, Dept. of Atmospheric Science, Colorado State University, Fort Collins, CO 80523.
E-mail: johnson@atmos.colostate.edu

tigated the organization of convection over the western Pacific warm pool using aircraft data from the Tropical Ocean Global Atmosphere Coupled Ocean–Atmosphere Response Experiment (TOGA COARE). In agreement with Alexander and Young (1992) they find that vertical shear in the low to midtroposphere is a key factor in determining the orientation of convective bands, while CAPE influences their depth and longevity. Their results have been recently supported by numerical simulations of convection in shear by Robe and Emanuel (2001).

The way in which convection organizes is important from several perspectives. First, it has an important effect on the vertical distribution of heating. For example, it is well known that convection that organizes perpendicular to the low-level shear vector often produces squall lines with extensive stratiform precipitation (Houze 1977; Zipser 1977), and that the corresponding latent heating profiles for the convective and stratiform components of squall systems can be quite different (Houze 1982, 1989; Johnson 1984). Systems containing extensive stratiform precipitation are characterized by a strong vertical gradient in the heating rate in the midtroposphere, whereas those consisting principally of deep convection do not. In addition, there is evidence to suggest that convective momentum transport is a function of system organization, with upgradient transport in the line-normal direction and downgradient transport in the line-parallel direction (LeMone 1983; Wu and Yanai 1994; Tung and Yanai 2002). Further, observations from COARE indicate that surface fluxes are greatly enhanced in convection that is highly organized and contains extensive stratiform precipitation areas as opposed to less organized convective systems (Saxen and Rutledge 1998). Finally, the extent of high clouds and cirrus associated with convective systems may depend on their organization, which would then influence the surface and tropospheric radiative fluxes.

Beyond the issue of convective organization, precipitation systems in the SCSMEX region have broadscale implications for the Asian monsoon. For example, Nitta (1987) has shown that convection over the SCS and the Philippines has major impacts on the summertime occurrence of droughts and floods over East Asia and Japan. These teleconnections are likely influenced by changes in the vertical distribution of heating that occur during the course of the monsoon. In addition, understanding the nature of precipitating systems in SCSMEX is significant because much of the world's heaviest rainfall in the monsoon regions occurs in similar near-coastal environments upstream of major landmasses [e.g., upstream of the Western Ghats, Myanmar, Sumatra; Hirose and Nakamura (2002); Adler et al. (2003)].

This study represents the first step in an investigation of the organization of convection in SCSMEX, as a precursor to subsequent study of the impacts of convective organization on the vertical distribution of heating in the East Asian monsoon. In this paper, we explore the relationship between convection and vertical wind shear using radar reflectivity data from the Bureau of Meteorology Research Centre (BMRC) 5-cm dual-polarization Doppler radar (C-Pol) on Dongsha Island in the northern SCS and proximity sounding data. The objective of this study is to determine whether the findings of Alexander and Young (1992) and LeMone et al. (1998) concerning the relationship between wind shear and convective organization in the Tropics can be extended to the oceanic monsoon region of SCSMEX, where both tropical and midlatitude influences exist.

2. Data and analysis procedures

a. Radar data

Ground-based radar data are obtained from the BMRC C-Pol radar, which was located at Dongsha Island (20.7°N, 116.7°E) in the northern SCS (Fig. 1). C-Pol was operational from 4 May to 21 June with several days of data gaps. However, the dataset is complete for the period of this study, 15–25 May. Animations of base-scan reflectivity fields at 10-min intervals over a 500 km × 500 km domain were used to determine the dominant organizational modes and propagation characteristics of the convection for 6-h periods. Six-hour periods were selected in part because soundings were launched at this interval. In addition, 6 h is long enough to capture a substantial fraction of the life cycle of organized convective systems, yet short enough to detect changes in convective organization frequently observed to occur in the region on a half-day time scale or less. In some instances, the environment did not change substantially from one 6-h period to the next, and the same organizatonal mode of convection persisted. In other cases, the environment was changing, and a specific

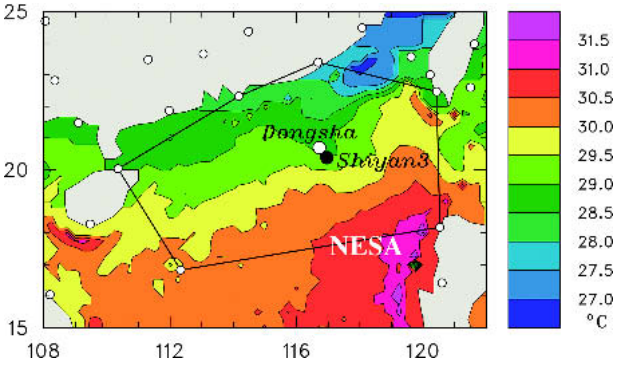

FIG. 1. SCSMEX/GAME sounding network (circles) and SST distribution (scale to right) for May–Jun 1998. The BMRC C-Pol radar was located on Dongsha Island, and 6-hourly soundings were taken at *Shiyan 3*. Sounding polygon NESA refers to Northern Enhanced Sounding Array.

mode of organization was difficult to detect or several modes coexisted. When there was no dominant mode of organization, the 6-h period was referred to as unclassifiable.

The fields of radar reflectivity were partitioned into convective and stratiform contributions using a modification of the horizontal texture-based procedure of Steiner et al. (1995, hereafter SHY95). The modification is patterned somewhat along the lines of Biggerstaff and Listemaa (2000), who used additional information on the vertical radar reflectivity structure to classify the character of precipitation. Our revised classification scheme is described in the appendix. As in Biggerstaff and Listemaa, the revised procedure reclassifies the periphery of convective cores from stratiform to convective, while heavy stratiform rainfall is reclassified from convective to stratiform. The net effect of our new procedure applied to the SCSMEX monsoon onset period is relatively small; namely, the stratiform rain fraction is increased over that given by SHY95 by about 4%.

b. Sounding data and surface data

The SCSMEX sounding network was contained within the larger domain of the Global Energy and Water Cycle Experiment (GEWEX) Asian Monsoon Experiment (GAME). Sounding sites in proximity to the C-Pol radar within the SCSMEX/GAME domain, along with the May–June 1998 mean sea surface temperature (SST), are shown in Fig. 1. During the intensive observing period (IOP; 5 May–20 June) of SCSMEX, these sounding sites typically had four sonde launches per day. The mean SST field was derived from daily values obtained from the Tropical Rainfall Measuring Mission (TRMM) Microwave Imager (TMI) SST product (Wentz et al. 2000). The C-Pol radar on Dongsha Island was located 40 km northwest of the R/V *Shiyan 3,* where 6-hourly Vaisala–GPS soundings were launched. The *Shiyan 3* soundings, rather than those at Dongsha Island, are used as proximity soundings for the convection in the C-Pol radar range since a single sounding type was used there (two sounding systems were used at Dongsha). Every effort was made to select soundings that were taken outside the convective areas to classify line organization, preferably in advance of the convective lines. However, with fixed sounding launch times, this was not always possible. Even soundings in the environment of convective systems can experience flow modification by convectively generated gravity waves (e.g., Nicholls et al. 1991; Mapes 1993), so (as in all studies of this nature) there may be some instances of contamination of the "ambient" flow by the convection itself. The sounding polygon in Fig. 1 is referred to as the northern enhanced sounding array or NESA. Sounding quality control procedures and other aspects of the sounding data analysis are described in Johnson and Ciesielski (2002). Surface data on Dongsha Island were obtained from automatic weather stations deployed there during SCSMEX by BMRC.

Figure 1 shows that a strong north–south SST gradient existed across the NESA during SCSMEX. Cooler waters near the south China coast, a residual of the winter monsoon, existed throughout the IOP, although the gradient weakened slightly throughout the period. Johnson and Ciesielski (2002) noted that the warmer waters to the south may have accounted for the positioning of the primary rainfall maximum away from the south China coastline during the onset period in mid-May. They also found that the tongue of cooler water extending through the Taiwan Straits toward *Shiyan 3* (Fig. 1) helped to reduce the surface fluxes at this location following monsoon onset as a southwesterly flow of warm, moist air passed over cooler water.

3. Evolution of the flow, convection, and precipitation during onset

The evolution of outgoing longwave radiation (OLR) and the 850-hPa zonal wind component accompanying the onset of the 1998 monsoon are shown in Fig. 2, as a Hovmöller diagram of those fields over the longitudes of the SCS. In early May the low-level flow over the SCS was easterly in association with the subtropical ridge to the north. A clear signal of southward propagation of high cloudiness into the northern SCS can be seen in mid-May and then into the central SCS near 10°N in late May (Chan et al. 2000; Ding and Liu 2001). The onset of westerlies was coincident with the arrival of high cloudiness. In June, both southward- and northward-propagating bands of convection can be inferred from Fig. 2, each accompanied by surges in the westerlies (Chang and Chen 1995; Chan et al. 2000).

A time series of precipitation rate over the NESA during the SCSMEX IOP is shown in Fig. 3. These results (from Johnson and Ciesielski 2002) are based on the moisture budget and the TRMM 3B42 combined-algorithm product (Kummerow et al. 2000). They show two ~10-day rainy periods separated by a break near the end of May. These independent estimates of rainfall rate agree rather well. This paper focuses on the first of these two rainy periods; the organization of convection during the second period will be the subject of a future study.

4. Mesoscale organization of convection during monsoon onset

Prior to the monsoon onset on 15 May, the low to midtroposphere was very dry and only scattered, shallow convective cells existed over the northern SCS. Following onset, convection increased, became organized on the mesoscale, and moistened the entire troposphere as the large-scale circulation changed to produce low-level convergence over the region (Chan et al.

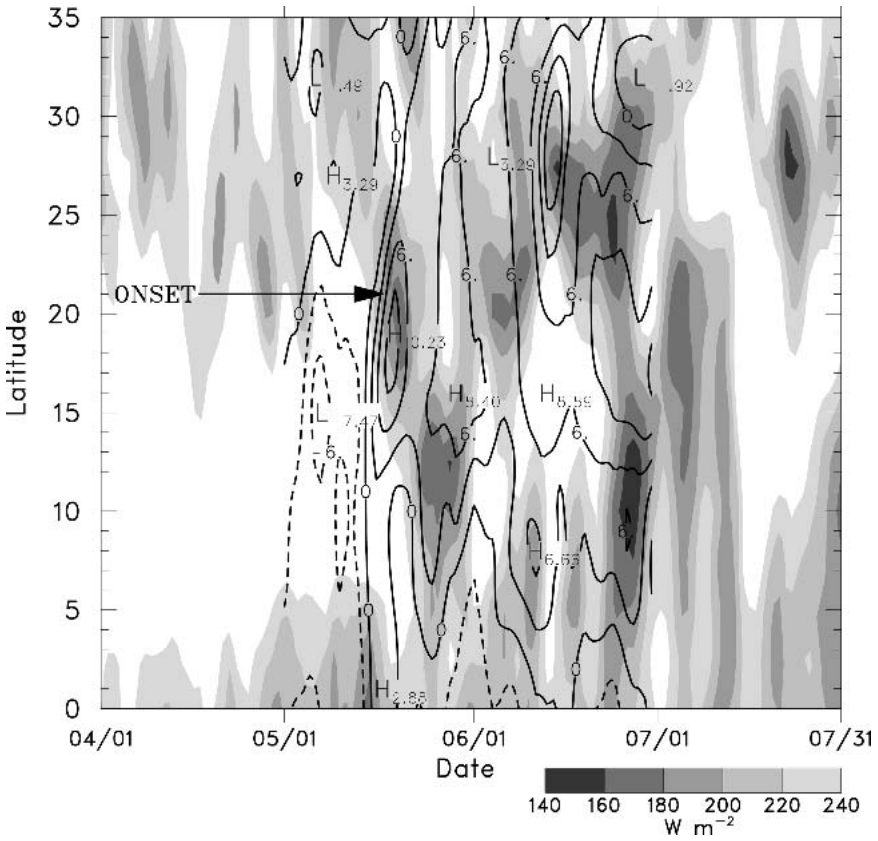

FIG. 2. Hovmöller diagram of OLR (shaded; scale at lower right) and zonal wind component u (m s^{-1}; westerlies, solid; easterlies, dashed) at 850 hPa between 110° and 120°E (South China Sea). Winds are shown for the May–Jun 1998 SCSMEX period. Convection associated with onset is noted.

2000; Ding and Liu 2001; Johnson and Ciesielski 2002). For a period of 11 days following monsoon onset (15–25 May), precipitation occurred continuously within the range of the radar, usually in bands but assuming a wide range of convective and stratiform patterns, band orientations, and lifetimes.

a. General classification

Animations of the C-Pol radar base-scan reflectivity within ~200 km radius of Dongsha Island were used to determine the dominant modes of convective organization at 6-h intervals (e.g., 0030–0900, 0900–1500 UTC, etc., centered at the 0600, 1200 UTC, etc., sounding times). Lines were classified as shear parallel (or shear perpendicular) if the line orientations were within 20° of specific shear vectors (or their perpendicular components) for the low and midtroposphere. Following LeMone et al. (1998), 1000–800 hPa was selected as the low-level shear layer, although this choice was slightly modified [using the procedure in Alexander and Young (1992)] when large hodograph curvature existed at the top or bottom of the layer in order to properly capture the dominant shear layer. As in Alexander and Young (1992) and LeMone et al. (1998), 800–400 hPa was selected as the nominal midlevel shear layer; however, there were some instances where bands parallel to the midlevel shear were more closely aligned along the midlevel shear vector for slightly different layers, for example, 700–400, 800–500 hPa, etc. Therefore, in practice, such bands were defined as shear parallel if they were within 20° of the shear vector for a layer 300 or

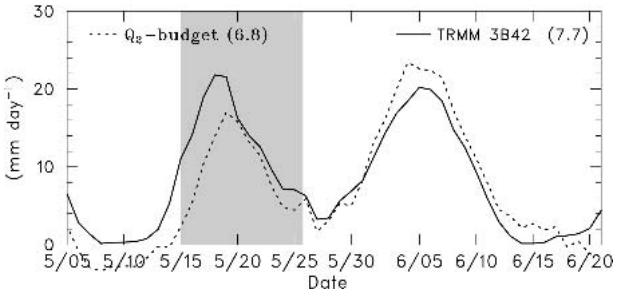

FIG. 3. Time series of rainfall rate (5-day running mean) from the moisture budget and TRMM 3B42 combined algorithm (Johnson and Ciesielski 2002). Mean values are in parentheses. Shaded area denotes period of study of convective organization.

400 hPa deep between 800 and 400 hPa. In addition, since the vertical shear likely varied horizontally over the radar domain on many occasions, the selection of bands for classification was done as often as possible in proximity to the sounding site used for the analysis at *Shiyan 3* (Fig. 1). Convective lines near the South China coast (300 km from *Shiyan 3*) often had different orientations (usually parallel to the coastline) than lines near *Shiyan 3,* reflecting the influence of coastal effects and low-level flow that was likely different in that location. Thus, classification was restricted to lines away from the South China coastline. As might be expected, classification of bands was not always unambiguous. When the organizational mode was uncertain, systems were labeled unclassifiable.

Based on thresholds for weak and strong low-and midlevel shears (4 m s^{-1} for the low-level shear layer and 5 m s^{-1} for the midlevel shear layer), four categories of convection emerged from the classification exercise (categories 1–4; Fig. 4). This figure, adapted from LeMone et al. (1998), is a summary of their findings from TOGA COARE, but supplemented by new results from SCSMEX (2r and 4c). One of the striking results from SCSMEX is the wide variety of organizational modes of convection observed during the onset of the summer monsoon. In general, the modes of convective organization during SCSMEX were consistent with those determined by LeMone et al. (1998) for the western Pacific warm pool. They found that when the shear in the lowest 200 hPa exceeded 4 m s^{-1} and the shear from 800 to 400 hPa was less than 5 m s^{-1}, the orientation of the primary convective band was perpendicular to the low-level shear (category 2 in Fig. 4). Secondary lines parallel to the low-level shear were found in some cases to be ahead of the primary band. In the absence of strong low-level shear, lines formed parallel to the 800–400-hPa shear when its magnitude exceeded 5 m s^{-1} (3 in lower-left panel of Fig. 4). When the vertical shear exceeded the thresholds in both layers and the shear vectors were not in the same direction (lower-right panel), the primary band was normal to the low-level shear (4a or 4b). Trailing secondary bands parallel to the midlevel shear occurred if the midlevel shear was opposite the low-level shear (4b). When the shear in both layers was weak, convection developed in arcs along outflow boundaries (1). The new modes 2r (moderately deep convective lines parallel to the low-level shear) and 4c (deep convective lines parallel to both the low- and midlevel shear) will be discussed in detail later.

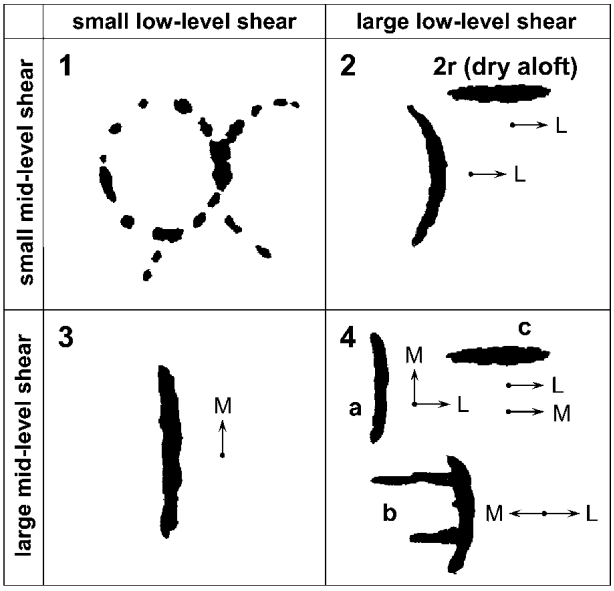

FIG. 4. Schematic depiction from LeMone et al. (1998) of four main categories of convective structures for given vertical shears in the lower troposphere (1000–800 hPa) and at middle levels (800–400 hPa) based on COARE observations, but modified to include results from SCSMEX (modes 2r and 4c added). Lengths of the schematic convective bands are ~100–300 km; line segments in upper-left panel are up to 50-km length. Cutoff between "strong" and "weak" shear for lower layer (1000–800 hPa) is 4 m s^{-1} and for middle layer (800–400 hPa) is 5 m s^{-1}. Arrows marked L and M are shear vectors for lower and middle layers, respectively. See text for descripition of convective modes.

b. Orientation and speed of convective lines

Characteristics of convective lines are presented in Table 1 for all cases studied. The table indicates the time, category, orientation of the main convective line (shear perpendicular or shear parallel), line orientation direction, shear direction and speed for the relevant layers, and the line speed (component of the line motion normal to the main convective line). All cases identified as shear perpendicular had the main convective line approximately perpendicular to the low-level shear vector. For shear-perpendicular cases, line orientation is defined as in Alexander and Young (1992) as the direction from which a vector directed from the left end to the right end of an approaching line points. Shear-parallel lines were parallel to the midlevel shear for 3's, the low-level shear for 2r's, and the shear in both layers for 4c's. For shear-parallel lines, line orientation is given by the direction within 20° of the shear vector for the relevant layer.

As seen from Table 1, most lines during the onset period were oriented northwest–southeast, the exceptions being an east–west line on 19 May and a group of lines on 24 and 25 May, which were oriented southwest–northeast. Plots of line orientations as a function of shear vectors, along with regression lines, for shear-perpendicular and shear-parallel lines are shown in Fig. 5. For the nine shear-perpendicular cases (Fig. 5a), near perpendicularity between line orientation and the low-level shear vector is evident. This finding is consistent with the idea that convection organizes to establish a balance between the cold pool and low-level shear when the low-level shear is sufficiently large or near

TABLE 1. Classification of line categories, defined in Fig. 4, at 6-h intervals (⊥, shear perpendicular; ||, shear parallel). Cases not fitting any of the modes in Fig. 4 are denoted as U, unclassifiable; I, isolated convection; and M, missing sounding data. Line orientation is defined as the direction from which a vector directed from the left end to the right end of an approaching line points. Directions and speeds of low and midlevel shears are given by the vector subtraction, top wind minus bottom wind, for the respective layers.

Date	Time (UTC)	Category	Line orientation	Low-level shear direction/speed (m s^{-1})	Midlevel shear direction/speed (m s^{-1})	Line speed (m s^{-1})
16 May	0000	4a (⊥)	120°	210°/6		6
	0600	4a (⊥)	130°	230°/10		7
	1200	2 (⊥)	150°	250°/9		7
	1800	U				
17 May	0000	3 (||)	310°		310°/12	8
	0600	U				
	1200	M				
	1800	2 (⊥)	160°	270°/5		7
18 May	0000	U				
	0600	2 (⊥)	150°	240°/5		8
	1200	2 (⊥)	150°	230°/8		8
	1800	4c (||)	290°	280°/7	270°/8	0
19 May	0000	M				
	0600	4a (⊥)	260°	350°/10	270°/19	4
	1200	U				
	1800	U				
20 May	0000	3 (||)	290°		300°/9	2
	0600	3 (||)	280°		270°/8	0
	1200	3 (||)	300°		300°/8	0
	1800	3 (||)	290°		280°/6	0
21 May	0000	U				
	0600	2r (||)	310°	300°/8		3
	1200	U				
	1800	U				
22 May	0000	I				
	0600	1				9
	1200	1				9
	1800	2r (||)	300°	300°/10		1
23 May	0000	2r (||)	310°	310°/10		0
	0600	2r (||)	310°	310°/5		0
	1200	2r (||)	310°	300°/8		0
	1800	2r (||)	300°	300°/8		0
24 May	0000	M				
	0600	I				
	1200	4b (⊥)	220°	320°/9	150°/10	10
	1800	U				
25 May	0000	4c (||)	210°	220°/9	200°/6	11
	0600	4a (⊥)	220°	290°/10	180°/7	4
	1200	4c (||)	210°	200°/8	200°/8	10
	1800	I				

"optimal" (Thorpe et al. 1982; Rotunno et al. 1988). If the shear becomes too large or "superoptimal," lines tend to rotate away from the direction orthogonal to the shear so as to preserve a near-optimal cross-line component of the shear (Emanuel 1986; Robe and Emanuel 2001). However, excessive low-level shears were not observed in SCSMEX; they were all $\leq$10 m s^{-1} (Table 1). For shear-perpendicular lines, there was considerable scatter in the line orientations. The shear-parallel cases were closely aligned with the midlevel shear (Table 1 and Fig. 5b) and most had line orientations and shears clustered between 270° and 330°, with two exceptions (4c) occurring at the end of the period.

As seen from Table 1, in addition to the shear-perpendicular and shear-parallel lines, there were two 1's; three cases of isolated convective cells, I; and nine cases of mesoscale convective systems with no clearly identifiable mode of organization, referred to as unclassifiable, U. On three occasions, marked M, the shear could not be computed at *Shiyan 3* due to missing sounding data. Over 10 days from 16 to 25 May, 25 of 37 six-hour periods when sounding data were not missing (68% of the cases) were classifiable in the shear categories of Fig. 4, and 24% were unclassifiable.

Consistent with past studies, the shear-perpendicular lines were *fast moving* (Barnes and Seickman 1984) with an average speed of 7 m s^{-1}, whereas the shear-parallel lines were *slow moving* with an average speed of 2.5 m s^{-1} (Table 1). If the three anomalously fast-moving shear-parallel lines of 17 and 25 May (to be discussed later) are removed from the latter group, the average speed of the shear-parallel lines decreases to

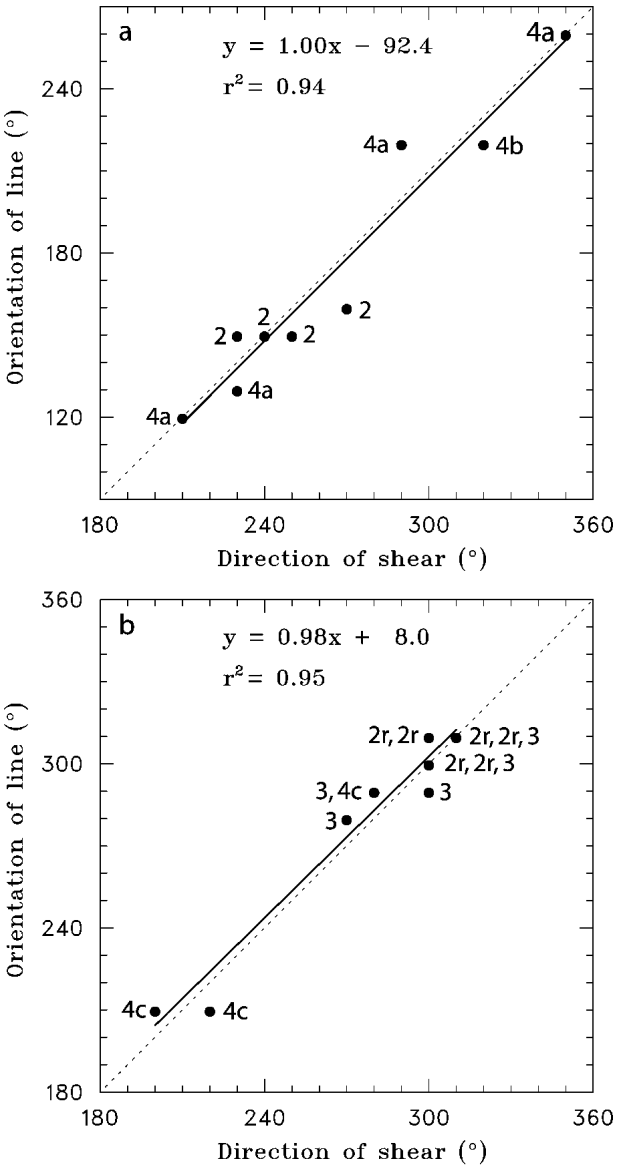

FIG. 5. (a) Line orientation as a function of low-level shear direction for nine category 2 and 4a,b shear-perpendicular convective lines. Most lines are oriented northwest–southeast, but two are oriented northeast–southwest. Solid line is a least squares fit to data points, dashed line is the exact shear-perpendicular direction, r is the correlation coefficient, and r^2 is the percent variance explained. (b) As in (a) except for 14 category 2r–3–4c shear-parallel convective lines. For categories 2r and 4c the shear direction is for the low-level shear; for category 3 it is the midlevel shear. Dashed line denotes exact shear-parallel direction.

0.4 m s^{-1}. The arc cloud lines in the 1 cases, presumably associated with outflow boundaries, moved at 9 m s^{-1}.

c. Thermodynamic and shear profiles

As noted earlier, LeMone et al. (1998) found that shear was the dominant factor influencing the orientation of convective lines, while CAPE influenced their depth and longevity. Similar findings hold for SCSMEX (although the lifetime of the SCSMEX lines could not be determined in all cases due to limited radar coverage). As reported by Wang (2004) and Tao et al. (2003), and discussed later, convective lines during the onset period were relatively weak and lacked extensive stratiform precipitation. This behavior may be related to the relatively low values of CAPE during the onset period. Figure 6 shows a time series of convective inhibition (CIN), CAPE, precipitable water (PW), and SST for a 2° × 2° box centered around *Shiyan 3.* The thermodynamic variables were computed from a 1° resolution objective analysis (Johnson and Ciesielski 2002). CAPE values on 15 May, when convection began, started off around 1200 J kg^{-1}, comparable to LeMone et al.'s (1998) mean value of 1470 J kg^{-1} for COARE, but then decreased to 400 J kg^{-1} by 25 May. CIN was relatively constant, but then increased toward the end of the period. CAPE was much larger prior to the onset of convection, but deep convection did not develop then due to dry conditions aloft, as suggested by PW time series in Fig. 6 and shown specifically by the time series of upper-tropospheric relative humidity in the bottom panel of Fig. 7. During the onset period, the passage of weak frontal systems from mainland China along with widespread precipitation downdrafts led to a gradual reduction of surface air temperature and specific humidity (Johnson and Ciesielski 2002), as well as SST (Fig. 6), which contributed to the pronounced reduction in CAPE through the period.

Time series of the vertical shears in the lower (1000–800 hPa) and middle (800–400 hPa) troposphere at *Shiyan 3* for 13–28 May are shown in Fig. 7. As noted earlier, 800–400 hPa was not always selected as the rel-

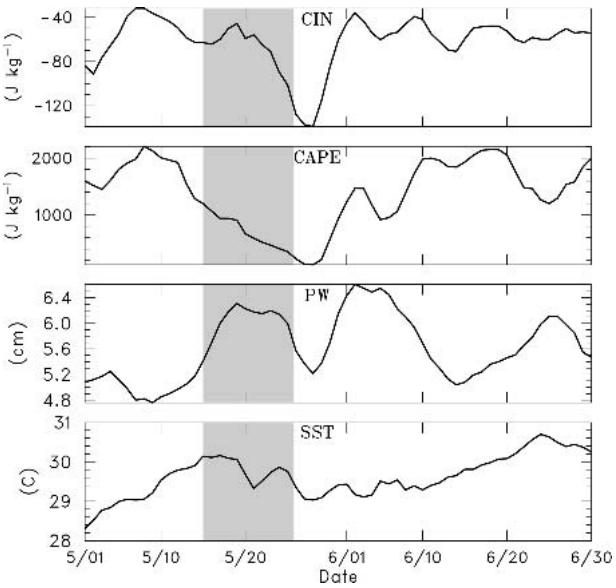

FIG. 6. Time series of 5-day running mean CIN, CAPE, PW, and SST for a 2° × 2° box centered near *Shiyan 3*. Shaded area denotes period of convective classification.

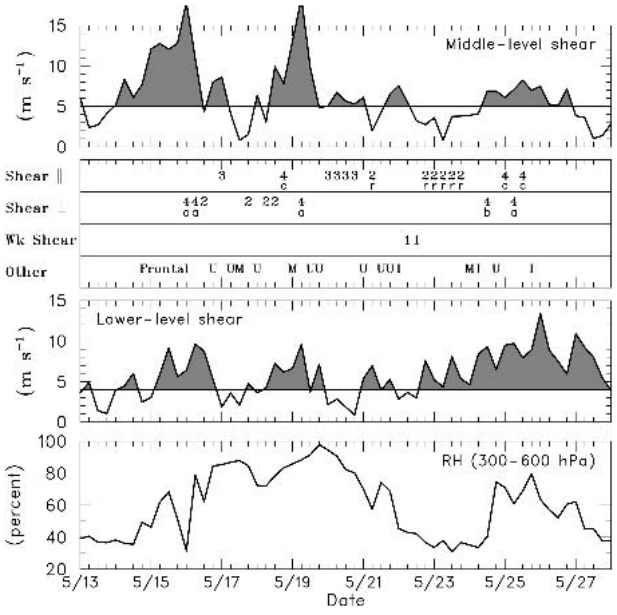

FIG. 7. Time series of shear vector magnitude in the low levels (1000–800 hPa) and middle levels (800–400 hPa), and 600–300-hPa relative humidity, based on 6-hourly sounding data from *Shiyan 3*. Periods with shear exceeding 5 m s^{-1} in the middle levels and 4 m s^{-1} in the lower levels are shaded. Convective organization in relation to the shear in the two layers is indicated in the second panel from the top, with numbers and letters referring to organizational modes depicted in Fig. 4. Those cases not fitting any of those modes are denoted as other: frontal, convection influenced by frontal system; U, unclassifiable; I, isolated convection; and M, missing sounding data. In the shear and relative humidity plots the three periods with missing *Shiyan 3* sonde data were filled in with large-scale analyses interpolated to the ship position.

evant midlevel shear layer; however, this plot is intended to provide a general overview of the midtropospheric shear throughout the early part of SCSMEX. There is an overall trend toward decreasing midlevel shear and increasing low-level shear as the transition to summer occurred, with a northward shift of the polar jet and a strengthening of the low-level monsoon flow. However, there was also considerable high-amplitude, short-term variability in the shear. Shading in Fig. 7 denotes periods when the shear exceeded thresholds defined by LeMone et al. (1998) for specific organizational modes of convection.

From Fig. 7 (second panel) and Table 1 it is evident that more times of shear-parallel than shear-perpendicular convective bands occurred over the northern SCS during the early monsoon onset period of SCSMEX (14 versus 9 cases). The results show that shear-perpendicular bands tended to occur when the low-level shear exceeded 4 m s^{-1}. As noted earlier, this finding is consistent with cold pool–low-level shear balance arguments. An exception occurred on 23 May when the midtroposphere became extremely dry (as seen in the 300–600-hPa mean relative humidity time series; bottom panel, Fig. 7), thus preventing deep convection and its associated downdrafts and cold pools and leading to shallow, shear-parallel lines. These lines are indicated by 2r in Fig. 4, where r indicates convection likely associated with longitudinal roll vortices in the boundary layer (Kuettner 1971; LeMone 1973; Christian and Wakimoto 1989). Isolated convective cells (I) also occurred during this period, likely due to a suppression of deep convection by the dry air aloft.

Another exception to the findings of LeMone et al. (1998) occurred when both the low and midlevel shears were strong but in the same direction, with shear-parallel bands occurring on three occasions (4c in Fig. 4). This behavior was also found in recent simulations by Robe and Emanuel (2001). The origin and nature of these bands are uncertain, but their alignment approximately along the low-level shear vector makes boundary layer rolls a candidate mechanism. This point was made for category 3 shear-parallel bands by LeMone et al. (1998). The 4c band on 18 May was nearly stationary, whereas the two on 25 May moved at about 10 m s^{-1}. However, in both of the latter cases the systems featured multiple convective lines quasi-parallel to the shear, and several instances of "jumps" or line reformation occurred to the east while individual lines moved to the east-northeast at 5 m s^{-1}. Similar "jumping" line behavior was observed in TOGA COARE (LeMone et al. 1998; Hildebrand 1998). The nearly stationary 4c band on 18 May resembles shear-parallel rainbands observed in the westerly monsoon flow north of Australia during the Equatorial Mesoscale Experiment (EMEX) (Houze 1989). The 25 May cases to some extent resemble prefrontal lines observed at midlatitudes ahead of cold fronts (e.g., Trier et al. 1991). A recent modeling study by Fovell and Kim (2003) suggests the origin of prefrontal bands may be from gravity waves generated by the convection ducted out ahead and triggering new lines ahead of old ones. It is possible that weak downdrafts for the 4c cases prevented shear-perpendicular bands from developing. LeMone et al. did not observe 4c cases in the TOGA COARE region, although Zipser et al. (1981) and LeMone (1983) did report such a case on 14 September 1974 in the eastern Atlantic during the Global Atmospheric Research Program (GARP) Atlantic Tropical Experiment (GATE).

More than half of the shear-perpendicular bands during the SCSMEX onset period were of the 4 variety since midlevel shear was also generally strong; however, four 2's also occurred. This control on convective organization (by strong midlevel shear) was influenced by the proximity of SCSMEX to the midlatitude westerlies, although this influence declined later in the period.

d. Individual cases

The first significant convection occurred on 15 May, but it was influenced by a frontal system that moved south from the southern China coast, leading to a sur-

face temperature drop of 4°C and a shift to a northeasterly wind at Dongsha Island. The convective band associated with the front can be seen in Fig. 8. The frontal contrast may have been aided by low-level convergence in the region of north–south SST gradient (Fig. 1), a frontogenetic situation. Convection after 15 May was mostly nonfrontal, although a shift to a northerly wind and some cooling occurred again on 19 May. In order to concentrate primarily on nonfrontal convection, classification of precipitation systems was restricted to the period 16–25 May.

Because the low-level flow was relatively strong throughout the period, only two cases of weak-shear events were observed (1's in Fig. 4). In these instances, convection was observed to develop in arcs along outflow boundaries.

Two varieties of the catgory 2 classification were observed during SCSMEX (strong low-level shear, weak midlevel shear). Four cases had shear-perpendicular primary bands. An example of a category 2 case (18 May) is shown in Fig. 9. The low-level shear vector [in this case taken from 975 to 800 hPa using the procedure of Alexander and Young (1992)] has been placed on the reflectivity plot. There is one primary band perpendicular to the low-level shear vector, while several bands ahead and behind are approximately parallel to it. It was followed several hours later by another shear-perpendicular primary band, the origins of which can be seen in the southwestern part of the domain. The primary band moved to the northeast at 8 m s^{-1}. The sounding shows relatively weak instability (CAPE = 792 J kg^{-1}) and very moist conditions up to 400 hPa. The coexistence of shear-perpendicular and shear-parallel bands suggests some bands are generating

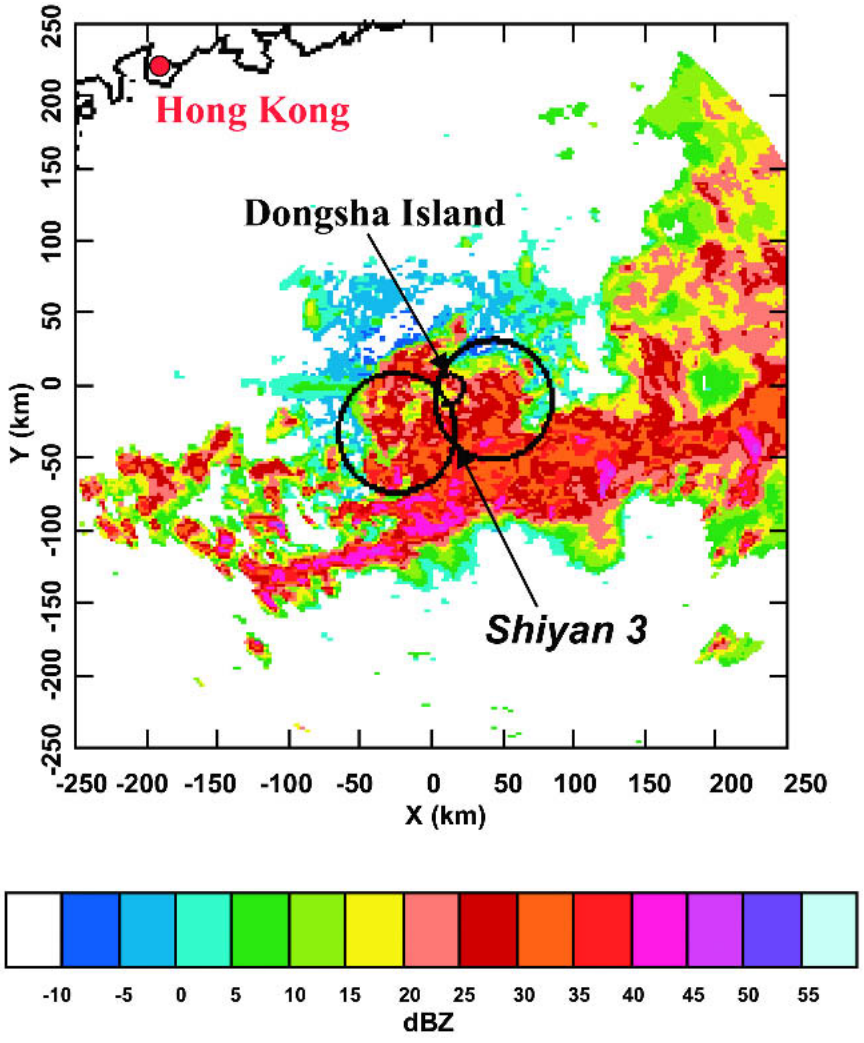

FIG. 8. Radar reflectivity (dBZ) from the C-Pol radar on Dongsha Island at 1129 UTC 15 May 1998. Intersecting circles are dual-Doppler lobes for C-Pol and TOGA radar (on *Shiyan 3*). As a cold front moved past the island near this time, the surface wind at Dongsha shifted to northeasterly and the temperature dropped by 4°C.

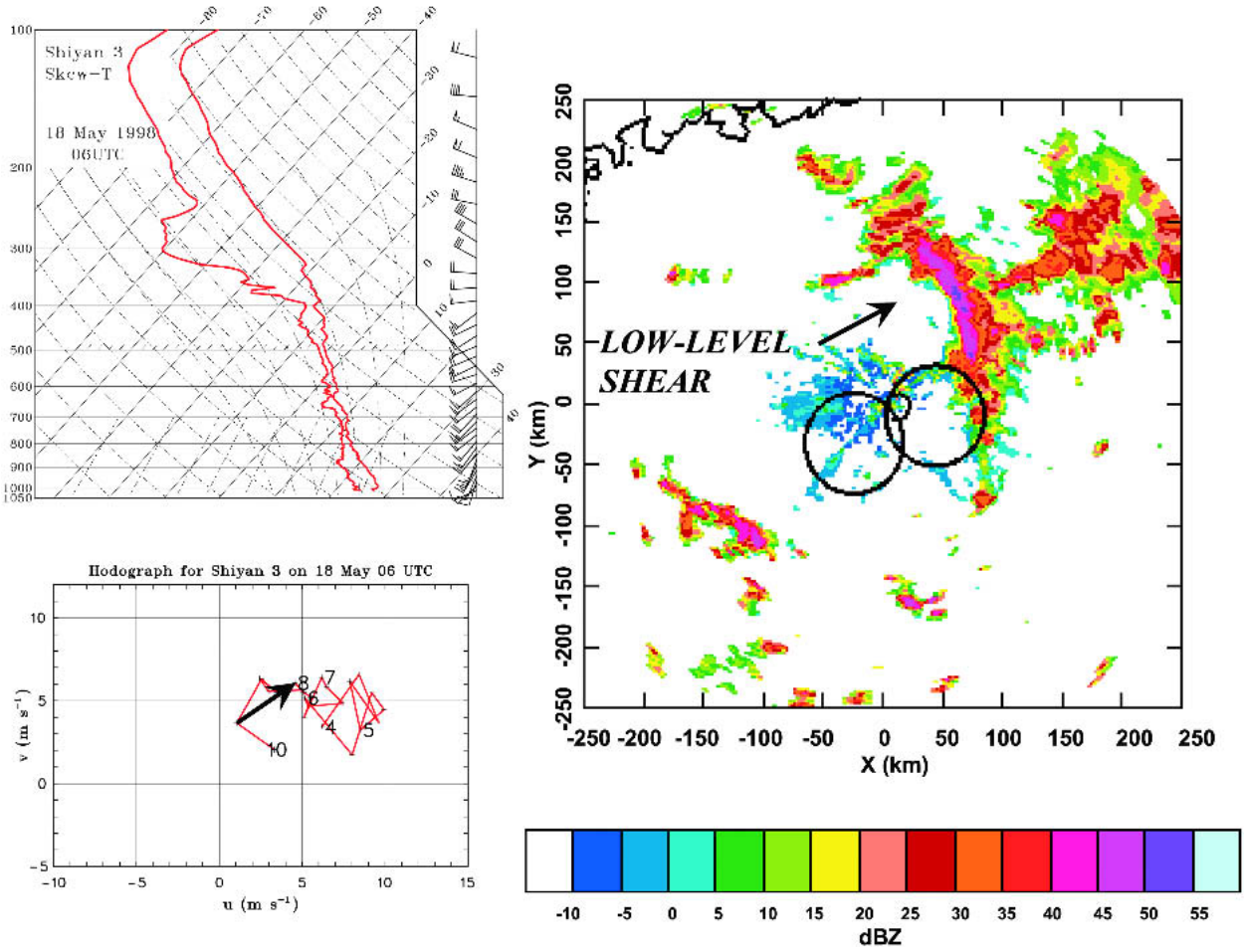

FIG. 9. *Shiyan 3* (top left) sounding and (bottom left) hodograph at 0600 UTC, and (right) C-Pol radar reflectivity at 0749 UTC 18 May 1998 for a category 2 case (strong low-level shear, weak midlevel shear, moist aloft: shear-perpendicular primary bands preceded by shear-parallel secondary bands). The low-level shear layer is 975–800 hPa. Line motion is to the northeast at 8 m s^{-1}. Hodograph extends from 1000 to 400 hPa; numbers indicate pressure level (e.g., 4 = 400 hPa).

strong cold polls and others are not. The temperature at Dongsha Island fell 3.5°C with the passage of the primary band, indicating a strong cold pool with that feature. The shear-parallel bands had weaker radar reflectivity and we speculate that they had weaker cold pools, such that their orientation was dictated more by the alignment of boundary layer horizontal convective rolls than cold pool–low-level shear interactions.

Interestingly, there was virtually no trailing stratiform precipitation with the primary band in the category 2 case. In fact, what little stratiform precipitation there was extended ahead of or in advance of the convective line, similar to the leading-stratiform (LS) precipitation system archetype identified at midlatitudes by Parker and Johnson (2000), and has been analyzed with radar data for other SCSMEX cases (Wang 2004). Parker and Johnson found that LS systems at midlatitudes (i) tend to move more slowly (~7 m s^{-1}) than their trailing-stratiform (TS) counterparts (~13 m s^{-1}) and (ii) have weaker front-to-rear (FTR) storm-relative flow at low levels than TS systems. Both aspects of LS systems reduce the likelihood for FTR storm-relative flow to develop aloft [in the case of (ii) through the vertical transport of weak FTR momentum from low levels to aloft]. With respect to the weak FTR flow at low levels, the primary band in this case was also relatively slow moving (8 m s^{-1}) and the surface southwesterly flow indicated weak FTR storm-relative flow at low levels.

By way of contrast, type 2r convection developed during a prolonged time of dry conditions aloft and weak instability. An example of this case, 23 May, is shown in Fig. 10.[1] The low-level shear layer is 950–800 hPa. Weak convective lines (reflectivities <40 dBZ)

[1]Humidity data were not available above 400 hPa at 1800 UTC, so the 1200 UTC sounding is shown; however, from Fig. 7 it can be seen that this entire period was dry aloft.

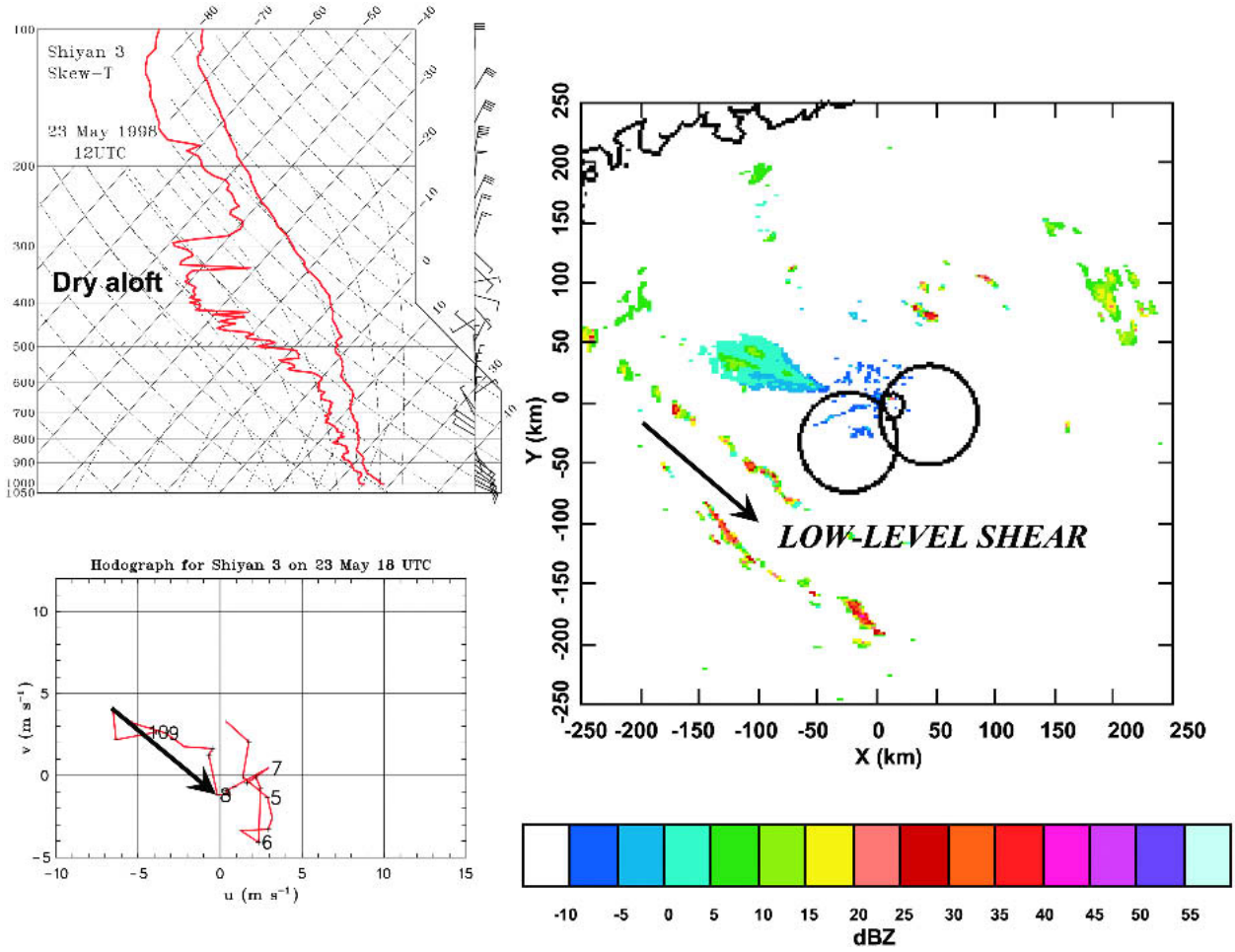

FIG. 10. *Shiyan 3* (top left) sounding and (bottom left) hodograph at 1200 UTC, and (right) C-Pol radar reflectivity at 1709 UTC 23 May 1998 for category 2r case (strong low-level shear, weak midlevel shear, dry aloft: weak shear-parallel bands). Data above 400 hPa in the 1800 UTC sounding are missing, so the 1200 UTC sounding is shown. Convective lines are stationary.

developed approximately parallel to the low-level shear vector. The spacing of these bands (~50 km) is much greater than the boundary layer depth, much like the cloud lines found by LeMone and Meitin (1984) in the trade wind boundary layer off Puerto Rico. Of course, additional rows of nonprecipitating clouds could have existed between the bands in Fig. 10. Such features, have been referred to as *wide mixed-layer rolls* by Young et al. (2002), to distinguish them from *narrow mixed-layer rolls* associated with individual longitudinal roll vortices. Possible explanations for the along-shear orientation of the bands offered by LeMone et al. (1998) are shear-modified Rayleigh instability as described by Asai (1970) or inertial, inflection-point or mixed-flow instability. However, there is no general consensus on the mechanisms for the spacing in the wide mixed-layer rolls. The occurrence of precipitation (from congestus clouds) in these bands indicates that latent heat release may have been a factor in their wide spacing (Young et al. 2002). The dry air aloft (Fig. 7, bottom) that capped the congestus clouds at this time was associated with ridging and subsidence following the passage of an upper-level trough, reflected in Fig. 7 as a weakening of the midlevel shear.

Evidence of the weaker convection in the 2r cases can be seen in Fig. 11, a plot of averaged vertical profiles of radar reflectivity for the various modes for grid points classified as convective. Only those convective modes where the population size is great enough to obtain a reasonable sample are included in Fig. 11. The profiles are similar for all except the 2r mode, which displays a much weaker reflectivity. This result is consistent with the observations for these cases showing much drier air aloft (Fig. 7), weak instability (Fig. 6), and hence shallower convective cells. The other convective reflectivity profiles are similar to those determined elsewhere in the Tropics (e.g., Szoke et al. 1986).

On five occasions, the midlevel shear was strong and the low-level shear was weak, contributing to shear-parallel or category 3 modes (Fig. 4). Most of these

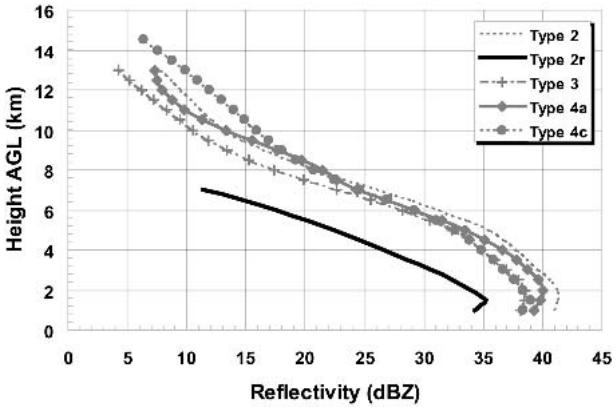

FIG. 11. Averaged vertical profiles of radar reflectivity for convective regions from the BMRC C-Pol radar for categories 2, 2r, 3, 4a, and 4c. Each vertical profile was truncated to exclude levels where the number of valid points is below 10% of the maximum number of points at any level.

bands were stationary or slow moving (Table 1), except for the ones on 17 May shown in Fig. 12. These bands (southwest of Dongsha Island) were closely aligned along the 700–400-hPa shear vector and moved toward the northeast at 8 m s^{-1}.[2] This motion is in contrast to the other cases as well as the slow-moving or nearly stationary shear-parallel rainbands observed in GATE (Zipser et al. 1981; LeMone 1983) and TOGA COARE (LeMone et al. 1998; Hildebrand 1998). However, some of the motion on 17 May took the form of discrete propagation or "jumps" as on at least one occasion a new line formed ahead of the previous one, as those authors also found. As this band passed Dongsha Island, there was a temperature drop of 2°C and a wind gust to 13 m s^{-1}. As noted by Zipser et al. (1981) in the

[2]The shore-parallel bands near the south China coastline existed in an environment with a different shear than that at *Shiyan 3,* as indicated by Hong Kong sounding data (not shown), and were likely influenced by coastal or land-breeze effects.

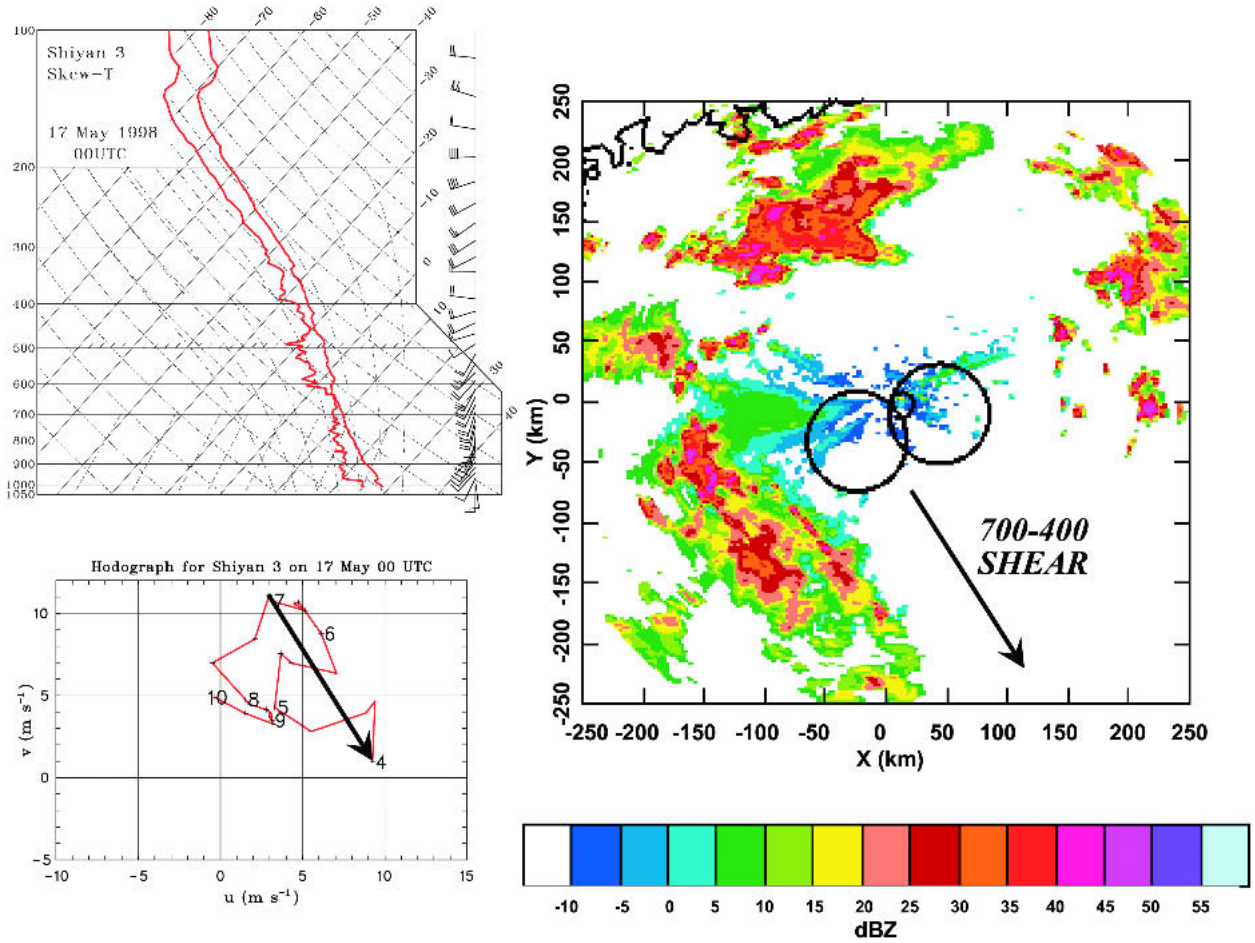

FIG. 12. *Shiyan 3* (top left) sounding and (bottom left) hodograph at 0000 UTC 17 May, and (right) C-Pol radar reflectivity at 2329 UTC 16 May 1998 for category 3 case (weak low-level shear, strong midlevel shear: shear-parallel bands). Convective bands southwest of Dongsha Island moved northeast at 8 m s^{-1}.

shear-parallel case they studied, temperature drops and wind gusts occur, but they tend to be smaller than those associated with typical (shear perpendicular) squall lines.

Three modes were observed when the shear was strong at both levels. The first type (category 4a) occurred on three occasions, with the primary bands perpendicular to the low-level shear and parallel to the midlevel shear. In the 16 May case (Fig. 13), two primary bands moved toward Dongsha Island at 7 m s^{-1}. The passage of the first was accompanied by a gradual temperature fall of 1.5°C over several hours. The second line weakened before arriving at Dongsha Island. As with the category 2 cases, there was very little stratiform precipitation associated with these bands.

There was only one category 4b event during the monsoon onset period, on 24 May (Fig. 14). The shear in the 700–400-hPa layer was approximately antiparallel to the 1000–800-hPa shear. LeMone et al. (1998) found that convection under these conditions is characterized by elongated secondary bands trailing and nearly perpendicular to the leading convective line, as in the case here. Lewis et al. (1998) found that such bands are supplied by moisture from low levels ahead of the squall line. In the TOGA COARE case they studied, Trier et al. (1997) determined that a similar secondary band had its origin in enhanced front-to-rear flow associated with a line-end vortex. The origin of the secondary bands on 24 May (a few of which appear ahead of the primary band) is uncertain owing to the lack of Doppler velocity data for this case. Somewhat similar behavior for reversed shear was found by Robe and Emanuel (2001), except their secondary bands were ahead of the primary band.

The final subcategory (4c), which occurred on three occasions, is characterized by strong shear in the low and midlevels in the same direction, nearly parallel to the alignment of the convective bands. This behavior is consistent with the simulations of Robe and Emanuel (2001). An example of this mode is shown in Fig. 15.

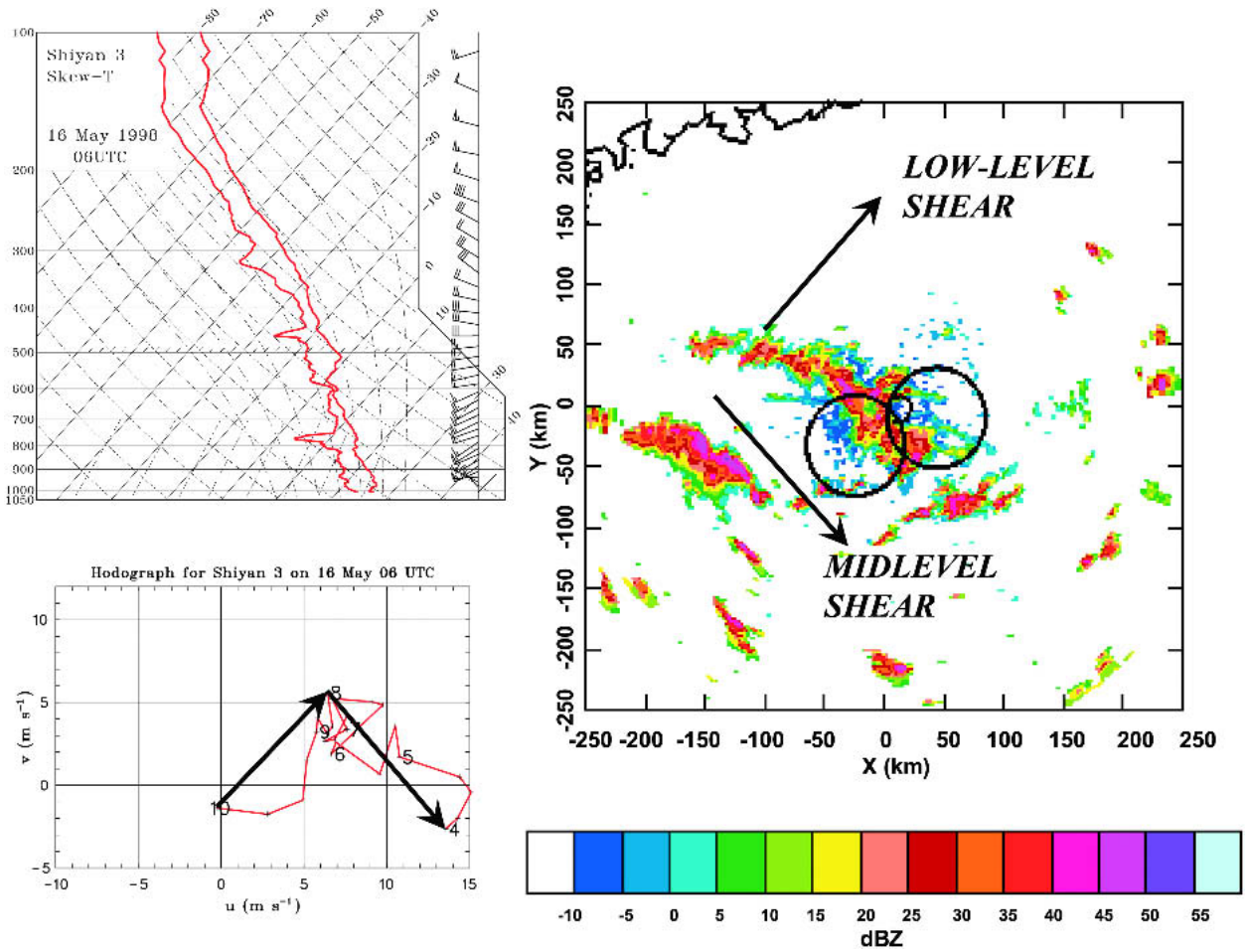

FIG. 13. *Shiyan 3* (top left) sounding and (top right) hodograph at 0600 UTC 16 May, and (right) C-Pol radar reflectivity at 0429 UTC 16 May 1998 for category 4a case (strong shear at low and midlevels, perpendicular-shear vectors: convection perpendicular to low-level shear, parallel to midlevel shear). Convective bands over and southwest of Dongsha Island moved northeast at 7 m s^{-1}.

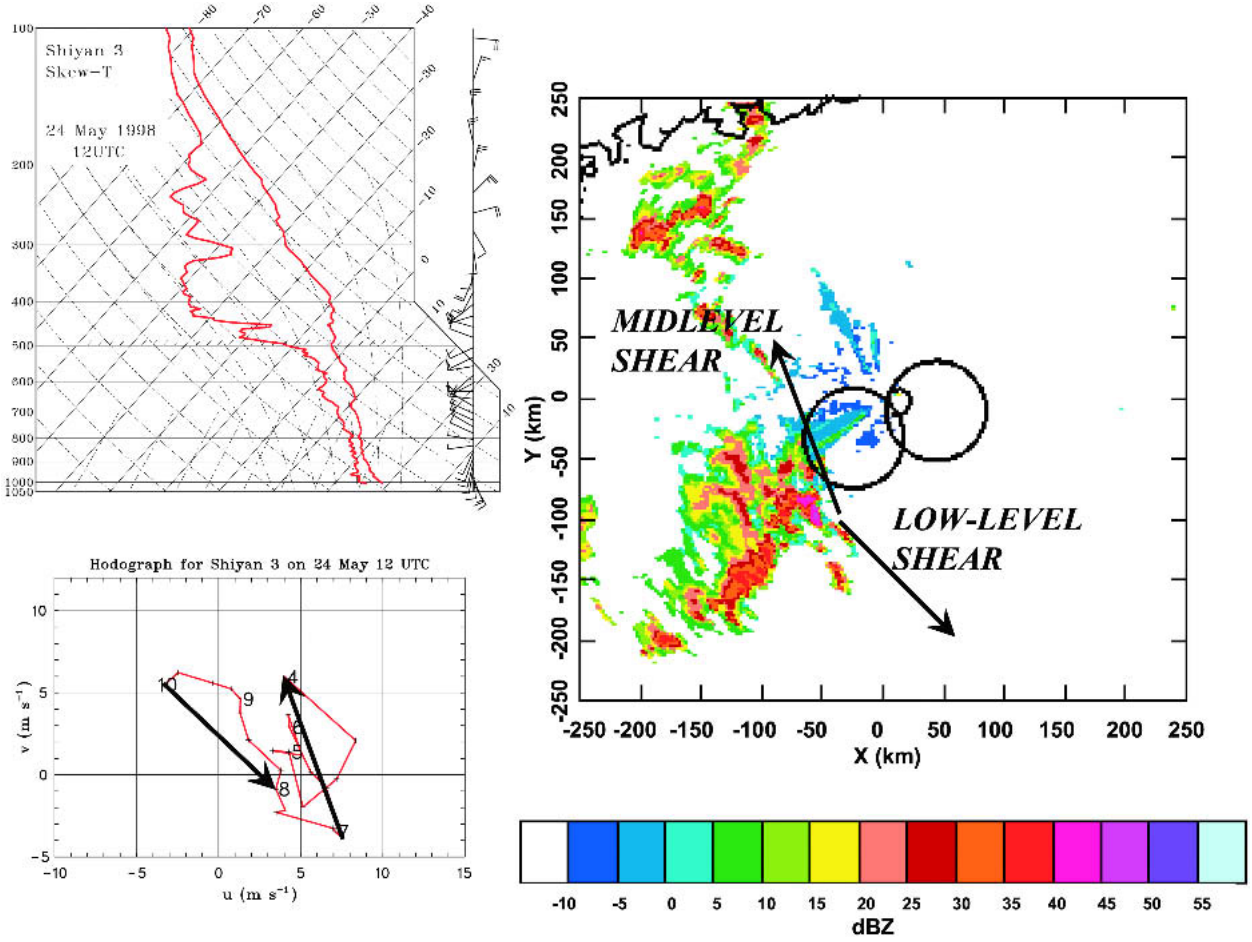

FIG. 14. *Shiyan 3* (top left) sounding and (bottom left) hodograph at 1200 UTC 24 May, and (right) C-Pol radar reflectivity at 1039 UTC 24 May 1998 for category 4b case (strong shear at low and midlevels; antiparallel vectors: main band perpendicular to low-level shear, trailing bands parallel to midlevel shear). Midlevel shear layer is from 700 to 400 hPa. Main convective band moved southeast at 10 m s^{-1}.

This case featured multiple convective lines quasi-parallel to the shear, and several instances of jumps or line reformation to the east while individual lines moved to the east-northeast at 5 m s^{-1}, similar to the category 3 system described above. Since in both cases the bands were quasi-parallel to the midlevel shear, it is possible that similar dynamics accounted for this behavior in both instances. LeMone (1983) identified a convection line on 14 September 1974 during GATE having characteristics similar to 4c. The 4c cases all occurred during the passage of 500-hPa troughs (not shown), which are reflected in Fig. 7 by increases in the midlevel shear. Another possible explanation for these bands is that they occurred along a deformation zone produced by the upper-level trough.

5. Stratiform rain fraction for the onset period

In most of the cases illustrated above, there was a notable lack of stratiform precipitation. Table 2 summarizes convective classification results for all of the cases. While the average areal percentage of stratiform precipitation for the entire period was 68%,[3] the percent stratiform rainfall was rather small (26%), a value much less than the average of about 40% often reported for tropical studies (Johnson and Houze 1987; Schumacher and Houze 2003). This low value is supported by the recent SCSMEX modeling results for the same period (Tao et al. 2003), wherein they found that much of the convection during the May onset period was "unicell" in nature, that is, it contained very little stratiform precipitation. Category 3 cases, which contribute the largest fraction of precipitation (30%), have the greatest percentage of stratiform rainfall (41%).

[3]This value is somewhat smaller than the 79% determined using the Steiner et al. (1995) procedure. The difference is principally due to a change in the classification of light rainfall areas on the periphery of convective cores from stratiform to convective by the modified procedure used in this study.

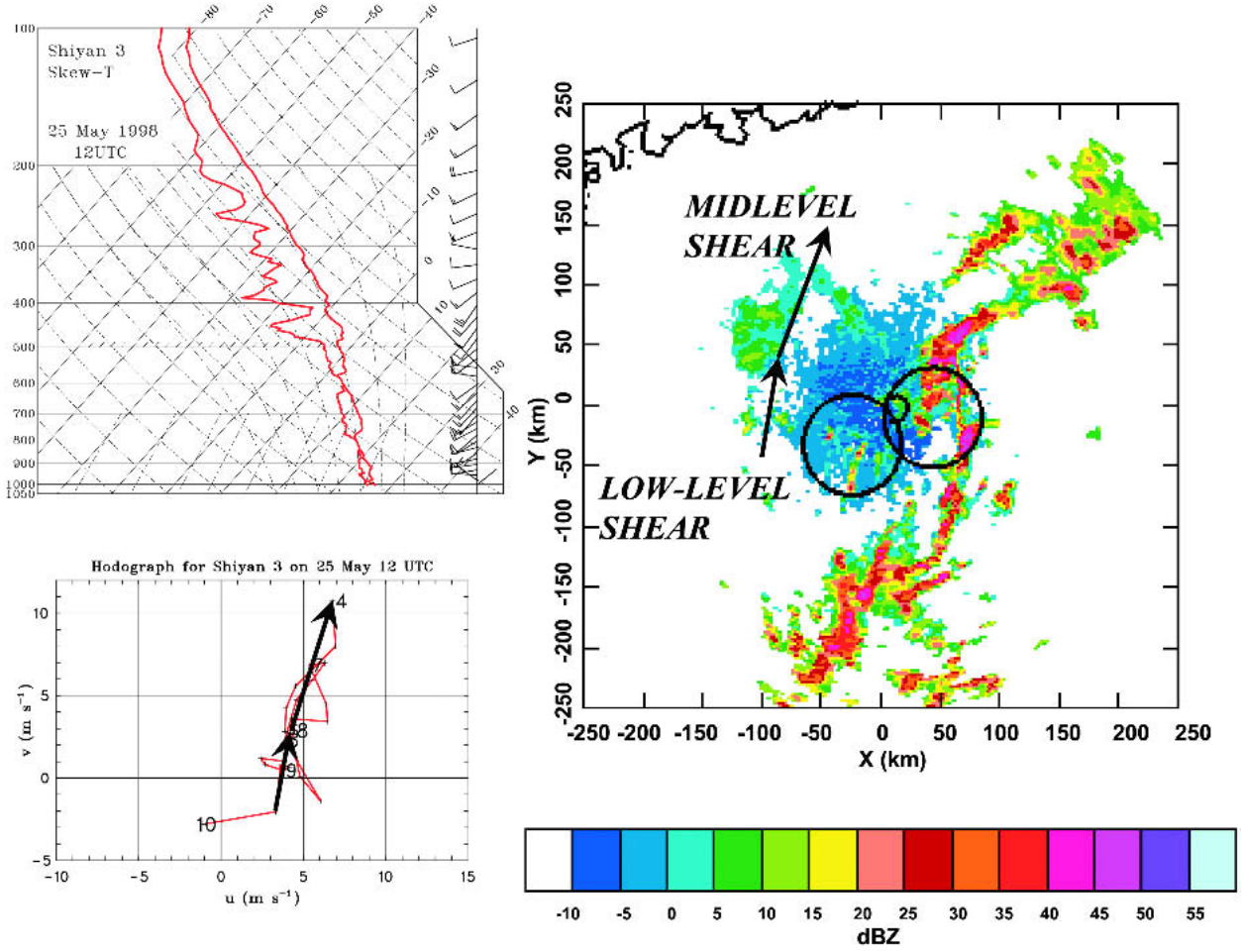

FIG. 15. *Shiyan 3* (top left) sounding and (bottom left) hodograph (lower left) at 1200 UTC 25 May, and (right) C-Pol radar reflectivity at 1129 UTC 25 May 1998 for category 4c case (strong shear at low and midlevels; parallel-shear vectors: convective bands parallel to shear at both levels). Low-level shear layer is from 975 to 800 hPa. Convective bands moved east-northeast at 5 m s^{-1}.

The reasons for this behavior are not yet understood. Given the limited number of cases, the extent to which this result can be generalized to other times and locations is not clear. It is well known that shear-perpendicular squall lines can often generate extensive stratiform precipitation regions, so the fact that they did not in this region during the monsoon onset may relect anomalous behavior. The small percentage of stratiform rainfall from 2r systems (9%) is consistent with the shallow character of these cloud systems (Fig. 11).

The relatively small stratiform rain fraction in SCSMEX convection during the monsoon onset can be attributed to several factors. First, values of CAPE during the onset period were relatively small ($\lesssim$1000 J kg^{-1} for much of the period) owing in part to precipitation downdrafts and the cool waters along the south coast of China (Johnson and Ciesielski 2002), thus limiting buoyancy in updrafts and the lofting of hydrometeors. Second, as is evident from Figs. 9, 10, and 14, the atmosphere over the northern SCS was frequently dry aloft, which would also inhibit the development of large stratiform anvils in the upper troposphere, a point also made by Wang (2004). An interesting question is whether the stratiform rain fraction increased during the early June rainy period (Fig. 3) when the SST and

TABLE 2. Stratiform rain contributions for all categories of convection. Stratiform area refers to the areal percentage of stratiform rainfall within a 150-km radius of the C-Pol radar, area (%) to the percent of the total area covered by each category, stratiform rain to the percent stratiform rainfall, and rain (%) to the percent of the total rainfall for each category.

Category	No. of cases	Stratiform area (%)	Area (%)	Stratiform rain (%)	Rain (%)
1	2	37	0.5	0.3	0.2
2	4	65	7.1	17	9.9
2r	6	42	6.8	9	4.2
3	5	81	39.0	41	30.4
4a	4	63	21.8	22	29.3
4b	1	55	2.1	10	2.5
4c	3	58	18.9	18	22.3
I	3	73	3.8	31	1.0
Total	28	68	100	26	100

CAPE increased. Mechanical failures of the C-Pol and TOGA radars (the latter aboard *Shiyan 3*) during much of the early June period preclude a thorough study of the stratiform rain fraction during that period; however, a few days of data are available and examination of those data is under way.

6. Summary and conclusions

The organization of convection over the northern South China Sea (SCS) has been investigated using BMRC C-Pol radar on Dongsha Island for the period 16–25 May 1998 during the South China Sea Monsoon Experiment (SCSMEX). The analysis focuses on convection over the open ocean away from the South China coastline to minimize coastal effects. The main results from this study are as follows:

- The lower- and middle-level vertical shears exerted a dominant control on the structure and orientation of mesoscale convective systems over the northern SCS during the monsoon onset period of SCSMEX, with both shear-parallel and shear-perpendicular modes of convection occurring over the 10-day period studied. Sixty-eight percent of the cases were classifiable, 24% unclassifiable, and 8% consisted of isolated convective cells. A striking result is the wide variety of organizational modes of convection in a monsoon flow environment.
- The organizational modes found during SCSMEX are consistent with those of LeMone et al. (1998) for TOGA COARE, except that two new modes have been identified: shear-parallel bands (2r in Fig. 10) for strong low-level shear and weak midlevel shear when the air was dry aloft, and shear-parallel bands (category 4c) for strong shears in both layers when the shear vectors were in the same direction (Fig. 15). Midlatitude influences likely contributed to these two additional modes by producing strong westerlies (in the case of category 4c) during the passage of upper-level troughs and midtropospheric drying (in the case of category 2r) as ridging ensued following passage of a trough.
- The stratiform rain fraction during the monsoon onset period was relatively small (26%) compared to the average of about 40% for the Tropics (Schumacher and Houze 2003). This small fraction is attributed to the weak instability during the onset period owing to low SSTs in the region, and relatively dry air in the upper troposphere.

A question of fundamental importance is why does convection respond the way it does to low- and midlevel wind shear? Answers to this question for some of the convective modes in Fig. 4 are generally understood. For example, category 2 modes are likely a consequence of the low-level shear perpendicular to the bands preventing the rain-produced, cold outflow from propagating rapidly away from the storm, consequently leading to a collocated gust front and updraft, and, hence, a long-lived storm (Thorpe et al. 1982; Rotunno et al. 1988). Similar arguments likely apply to the primary, shear-perpendicular convective lines in the 4a and 4b cases. The 2r shear-parallel bands appear to be linked to boundary layer roll vortices (Etling and Brown 1993; Young et al. 2002), where small instability and dry air aloft have limited the growth of convection to the extent that very weak, if any, cold pools are created. Less certain are the mechanisms for the shear-parallel 3 and 4c modes. LeMone et al. (1998) point out that cause(s) of category 3 events are unclear, and while Robe and Emanuel (2001) were able to simulate shear-parallel 4c bands, they do not provide an explanation for their orientation. Clearly, more work is needed on this problem.

This findings of this study are based on a limited number of cases, and caution must be exercised in generalizing the results to other times and locations. Nevertheless, the findings are consistent with those of Alexander and Young (1992) and LeMone et al. (1998), suggesting that wind shear in the low and midtroposphere organizes convection in the subtropics in a similar way as in the Tropics. Considering the impacts of convective organization on latent heating profiles, boundary layer modification, surface fluxes, convective momentum transport, and cirrus cloud distribution, understanding of large-scale controls on such organization has potentially important implications for both regional and general circulation models. Further work is now under way to investigate the latent heating profiles of the SCSMEX convective systems as a function of their organization.

Acknowledgments. This research has been supported by the National Aeronautics and Space Administration under Grant NAG5-9665. We thank Michael Whimpey of BMRC for providing C-POL radar data and for helpful discussions, Chelle Gentemann for providing the TMI SST data, Brian McNoldy and Rick Taft for assistance with preparation of the figures, and two anonymous reviewers for helpful comments on the manuscript.

APPENDIX

Convective–Stratiform Partitioning Procedure

The procedure to separate convective and stratiform precipitation is based on the approaches of Steiner et al. (1995, hereafter SHY95) and Biggerstaff and Listemaa (2000). The technique initially assumes all points to be stratiform by default, and then attempts to classify points as convective by comparing their horizontal and vertical radar reflectivity profiles to characteristics statistically derived by considering all of the points in the radar dataset that do not exhibit brightband signatures. Similar to SHY95, the algorithm first searches for con-

vective centers, which are defined as points whose reflectivity values exceed their background reflectivity by a given threshold. The background reflectivity is the logarithmic average of the reflectivities within 11 km of the point under consideration. The scheme developed for this study additionally requires that for a grid point to be classified convective, the level of maximum reflectivity should be below 3.5 km. Stratiform precipitation has a brightband signature with a reflectivity maximum above this level.

For each convective center, all points within two radii r_1 and r_2, whose lengths depend upon the reflectivity of the convective center, are considered for convective classification. Within r_1, whose size ranges from 2 to 5 km, data points with the characteristics of convective cores (reflectivity $\geq$40 dBZ and/or brightband fraction $\leq$0.5) are classified as convective. Here, brightband fraction is calculated as the fraction of points within a 7 km $\times$ 7 km box surrounding the point under consideration that exhibit a reflectivity maximum within 1.5 km of the freezing level (Rosenfeld et al. 1995). Within the larger convective fringe radius r_2, which ranges from 4 to 10 km, data points with the characteristics of convective core fringe points (no brightband signature in the vertical profile, brightband fraction $\leq$0.5, and 3–5 km AGL vertical reflectivity lapse rate ≤ -1.5 dBZ km) are also classified as convective. The latter criterion is based on observations that convective reflectivity profiles in this layer below the melting level (near 5 km) typically fall off rather rapidly (e.g., Fig. 11). Finally, a smoothing routine is executed to ensure spatial continuity.

REFERENCES

Adler, R. F., C. Kummerow, D. Bolvin, S. Curtis, and C. Kidd, 2003: Status of TRMM monthly estimates of tropical precipitation. *Cloud Systems, Hurricanes, and the Tropical Rainfall Measuring Mission (TRMM): A Tribute to Dr. Joanne Simpson, Meteor. Monogr.,* No. 51, Amer. Meteor. Soc., 223–234.

Alexander, G. D., and G. S. Young, 1992: The relationship between EMEX mesoscale precipitation feature properties and their environmental characteristics. *Mon. Wea. Rev.,* **120,** 554–564.

Asai, T., 1970: Thermal instability of a plane parallel flow with variable vertical shear and unstable stratification. *J. Meteor. Soc. Japan,* **48,** 129–139.

Barnes, G. M., and K. Seickman, 1984: The environment of fast- and slow-moving tropical mesoscale convective cloud lines. *Mon. Wea. Rev.,* **112,** 1782–1794.

Biggerstaff, M. I., and S. A. Listemaa, 2000: An improved scheme for convective/stratiform echo classification using radar reflectivity. *J. Appl. Meteor.,* **39,** 2129–2150.

Chan, J. C. L., Y. Wang, and J. Xu, 2000: Dynamic and thermodynamic characteristics associated with the onset of the 1998 South China Sea summer monsoon. *J. Meteor. Soc. Japan,* **78,** 367–380.

Chang, C.-P., and G. T.-J. Chen, 1995: Tropical circulations associated with southwest monsoon onset and westerly surges over the South China Sea. *Mon. Wea. Rev.,* **123,** 3254–3267.

Christian, T. W., and R. M. Wakimoto, 1989: The relationship between radar reflectivities and clouds associated with horizontal roll convection on 8 August 1982. *Mon. Wea. Rev.,* **117,** 1530–1544.

Ding, Y.-H., and Y. Liu, 2001: Onset and evolution of the summer monsoon over the South China Sea during SCSMEX field experiment in 1998. *J. Meteor. Soc. Japan,* **79,** 255–276.

Emanuel, K. A., 1986: Some dynamical aspects of precipitating convection. *J. Atmos. Sci.,* **43,** 2183–2198.

Etling, D., and R. A. Brown, 1993: Roll vortices in the planetary boundary layer: A review. *Bound.-Layer Meteor.,* **65,** 215–248.

Fovell, R. G., and S.-H. Kim, 2003: Discrete propagation in numerically simulated nocturnal squall lines. Preprints, *10th Conf. on Mesoscale Processes,* Portland, OR, Amer. Meteor. Soc., CD-ROM, 4.8.

Hildebrand, P. H., 1998: Shear-parallel moist convection over the tropical ocean: A case study from 18 February 1993 TOGA COARE. *Mon. Wea. Rev.,* **126,** 1952–1976.

Hirose, M., and K. Nakamura, 2002: Spatial and seasonal variation of rain profiles over Asia observed by spaceborne precipitation radar. *J. Climate,* **15,** 3443–3458.

Houze, R. A., Jr., 1977: Structure and dynamics of a tropical squall-line system observed during GATE. *Mon. Wea. Rev.,* **105,** 1540–1567.

——, 1982: Cloud clusters and large-scale vertical motion in the tropics. *J. Meteor. Soc. Japan,* **60,** 396–410.

——, 1989: Observed structure of mesoscale convective systems and implications for large-scale heating. *Quart. J. Roy. Meteor. Soc.,* **115,** 425–461.

——, S. G. Geotis, F. D. Marks, and A. K. West, 1981: Winter monsoon convection in the vicinity of north Borneo. Part I: Structure and time variation of the clouds and precipitation. *Mon. Wea. Rev.,* **109,** 1595–1614.

Johnson, R. H., 1984: Partitioning tropical heat and moisture budgets into cumulus and mesoscale components: Implications for cumulus parameterization. *Mon. Wea. Rev.,* **112,** 1590–1601.

——, and D. C. Kriete, 1982: Thermodynamic and circulation characteristics of winter monsoon tropical mesoscale convection. *Mon. Wea. Rev.,* **110,** 1898–1911.

——, and R. A. Houze Jr., 1987: Precipitating cloud systems of the Asian monsoon. *Monsoon Meteorology,* Vol. X, C.-P. Chang and T. N. Krishnamurti, Eds., Oxford University Press, 298–353.

——, and P. E. Ciesielski, 2002: Characteristics of the 1998 summer monsoon onset over the northern South China Sea. *J. Meteor. Soc. Japan,* **80,** 561–578.

Keenan, T. D., and R. E. Carbone, 1992: A preliminary morphology of precipitation systems in tropical northern Australia. *Quart. J. Roy. Meteor. Soc.,* **118,** 283–326.

Kuettner, J. P., 1971: Cloud bands in the earth's atmosphere: Observations and theory. *Tellus,* **23,** 404–426.

Kummerow, C., and Coauthors, 2000: The status of the Tropical Rainfall Measuring Mission (TRMM) after two years in orbit. *J. Appl. Meteor.,* **39,** 1965–1982.

Lau, K.-M., and Coauthors, 2000: A report of the field operations and early results of the South China Sea Monsoon Experiment (SCSMEX). *Bull. Amer. Meteor. Soc.,* **81,** 1261–1270.

LeMone, M. A., 1973: The structure and dynamics of horizontal roll vortices in the planetary boundary layer. *J. Atmos. Sci.,* **30,** 1077–1091.

——, 1983: Momentum transport by a line of cumulonimbus. *J. Atmos. Sci.,* **40,** 1815–1834.

——, and R. J. Meitin, 1984: Three examples of fair-weather mesoscale boundary-layer convection in the Tropics. *Mon. Wea. Rev.,* **112,** 1985–1998.

——, E. J. Zipser, and S. B. Trier, 1998: The role of environmental shear and thermodynamic conditions in determining the structure and evolution of mesoscale convective systems during TOGA COARE. *J. Atmos. Sci.,* **55,** 3493–3518.

Lewis, S. A., M. A. LeMone, and D. P. Jorgensen, 1998: Evolution

and dynamics of a late-stage squall line that occurred on 20 February 1993 during TOGA COARE. *Mon. Wea. Rev.,* **126,** 3189–3212.

Mapes, B. E., 1993: Gregarious tropical convection. *J. Atmos. Sci.,* **50,** 2026–2037.

Moncrieff, M. W., and J. S. A. Green, 1972: The propagation and transfer properties of steady convective overturning in shear. *Quart. J. Roy. Meteor. Soc.,* **98,** 336–352.

Nicholls, M. E., R. A. Pielke, and W. R. Cotton, 1991: Thermally forced gravity waves in an atmosphere at rest. *J. Atmos. Sci.,* **48,** 1869–1884.

Nitta, T., 1987: Convective activities in the tropical western Pacific and their impact on the Northern Hemisphere summer circulation. *J. Meteor. Soc. Japan,* **65,** 373–390.

Parker, M. D., and R. H. Johnson, 2000: Organizational modes of midlatitude mesoscale convective systems. *Mon. Wea. Rev.,* **128,** 3413–3436.

Robe, F., and K. A. Emanuel, 2001: The effect of vertical wind shear on radiative–convective equilibrium states. *J. Atmos. Sci.,* **58,** 1427–1445.

Rosenfeld, D., E. Amitai, and D. B. Wolff, 1995: Classification of rain regimes by the three-dimensional properties of reflectivity fields. *J. Appl. Meteor.,* **34,** 198–211.

Rotunno, R., J. B. Klemp, and M. L. Weisman, 1988: A theory for strong, long-lived squall lines. *J. Atmos. Sci.,* **45,** 463–485.

Saxen, T. R., and S. A. Rutledge, 1998: Surface fluxes and boundary layer recovery in TOGA COARE. *J. Atmos. Sci.,* **55,** 2763–2781.

Schumacher, C., and R. A. Houze Jr., 2003: Stratiform rain in the Tropics as seen by the TRMM precipitation radar. *J. Climate,* **16,** 1739–1756.

Steiner, M., R. A. Houze Jr., and S. E. Yuter, 1995: Climatological characterization of three-dimensional storm structure from operational radar and rain gauge data. *J. Appl. Meteor.,* **34,** 1978–2007.

Szoke, E. J., E. J. Zipser, and D. P. Jorgensen, 1986: A radar study of convective cells in mesoscale systems in GATE. Part I: Vertical profile statistics and comparison with hurricanes. *J. Atmos. Sci.,* **43,** 182–198.

Tao, W.-K., C.-L. Shie, J. Simpson, S. Braun, R. H. Johnson, and P. E. Ciesielski, 2003: Convective systems over the South China Sea: Cloud-resolving model simulations. *J. Atmos. Sci.,* **60,** 2929–2956.

Thorpe, A. J., M. J. Miller, and M. W. Moncrieff, 1982: Two-dimensional convection in nonconstant shear: A model of midlatitude squall lines. *Quart. J. Roy. Meteor. Soc.,* **108,** 739–762.

Trier, S. B., D. B. Parsons, and J. H. E. Clark, 1991: Environment and evolution of a cold-frontal mesoscale convective system. *Mon. Wea. Rev.,* **119,** 2429–2455.

——, W. C. Skamarock, and M. A. LeMone, 1997: Structure and evolution of the 22 February 1993 TOGA COARE squall line: Organization mechanisms inferred from numerical simulation. *J. Atmos. Sci.,* **54,** 386–407.

Tung, W.-W., and M. Yanai, 2002: Convective momentum transport observed during the TOGA COARE IOP. Part I: General features. *J. Atmos. Sci.,* **59,** 1857–1871.

Wang, J.-J., 2004: Evolution and structure of the mesoscale convection and its environment: A case study during the early onset of southeast Asian summer monsoon. *Mon. Wea. Rev.,* **132,** 1104–1120.

Wentz, F. J., C. Gentemann, D. Smith, and D. Chelton, 2000: Satellite measurements of sea surface temperature through clouds. *Science,* **288,** 847–850.

Wu, X., and M. Yanai, 1994: Effects of vertical wind shear on the cumulus transport of momentum: Observations and parameterization. *J. Atmos. Sci.,* **51,** 1640–1660.

Young, G. S., D. A. R. Kristovich, M. R. Hjelmfelt, and R. C. Foster, 2002: Rolls, streets, waves, and more. *Bull. Amer. Meteor. Soc.,* **83,** 997–1013.

Zipser, E. J., 1977: Mesoscale and convective-scale downdrafts as distinct components of squall-line circulation. *Mon. Wea. Rev.,* **105,** 1568–1589.

——, R. J. Meitin, and M. A. LeMone, 1981: Mesoscale motion fields associated with a slowly moving GATE convective band. *J. Atmos. Sci.,* **38,** 1725–1750.